Investigation of the Effect of Acquisition Schemes on Time-Resolved Magnetic Resonance Fingerprinting

Tian Li[1], Di Cui[2], Ge Ren[1], Edward S. Hui[3], Jing Cai[1]

1 – Department of Health Technology and Informatics, The Hong Kong Polytechnic University, Hong Kong

2- Department of Diagnostic Radiology, The University of Hong Kong, Hong Kong

3- Department of Rehabilitation Science, The Hong Kong Polytechnic University, Hong Kong

Abstract

Purpose: This study aims to investigate the feasibility of different acquisition methods for time-resolved magnetic resonance fingerprinting (TR-MRF) in computer simulation.

Methods: Extended cardiac-torso (XCAT) phantom is used to generate abdominal T1, T2, and proton density (PD) maps for MRF simulation. The simulated MRF technique consists of an IR-FISP MRF sequence with spiral trajectory acquisition. MRF maps were simulated with different number of repetitions from 1 to 15. Three different methods were used to generate TR-MRF maps: 1) continuous acquisition without delay between MRF repetitions; 2) continuous acquisition with 5 seconds delay between MRF repetitions; 3) triggered acquisition with variable delay between MRF repetitions to allow the next acquisition to start at different respiration phase. After the generation of TR-MRF maps, the image quality indexes including absolute T1 and T2 value, signal-to-noise-ratio (SNR), tumor-to-liver contrast-to-noise ratio (CNR), error in the amplitude of diaphragm motion and tumor volume error were used to evaluate the reconstructed parameter maps. Three volunteers were recruited to test the feasibility of the selected acquisition method.

Results: Dynamic MR parametric maps using three different acquisition methods were estimated. The overall and liver T1 value error, liver SNR in T1 and T2 maps, and tumor SNR from T1 maps from triggered method is statistically significantly better than the other two methods (p-value < 0.05). The other image quality indexes have no significant difference between the triggered method and the other two continuous acquisition methods. All image quality indexes exhibit no significant difference between the acquisition methods with 0 second and 5 seconds delay. The triggered method was successfully performed in three healthy

volunteers.

Conclusion: TR-MRF technique was investigated using three different acquisition methods in computer simulation where the triggered method showed better performance than the other two methods. The triggered method has been tested successfully in healthy volunteers.

1. Introduction

Liver cancer is the leading cause of cancer morbidity and mortality, especially in east Asia.[1] Among the various treatment options for liver cancer, radiation therapy has been drawing increasing attention recently. Several studies have reported promising results of using radiation therapy and stereotactic body radiation therapy (SBRT) for the treatment of inoperable liver cancer.[2-5] However, cautions must be taken when delivering the desired radiation dose to the target tumor such that the remaining healthy liver is spared from over-dosing because SBRT toxicity is still of a great concern.[6] There are several procedures that can help achieve a conformal radiation dose distribution to the target including high quality imaging for target delineation, accurate motion measurement, efficient motion management modalities, accurate dose calculation algorithms, high-spatial precision treatment delivery systems, and etc.[7-9] Among these procedures, tumor delineation and motion quantification are vital to the determination of tumor margin for the planning of radiation therapy. Inaccurate margin prescription could lead to radiation over-dose in healthy tissue or under-dose in tumor. A large margin is usually applied in traditional free breathing radiation therapy to account for the uncertainties in tumor delineation and motion.

It is therefore imperative that methods for precise tumor delineation and motion quantification be developed so that the margin can be reduced and more healthy tissue could be spared. Four-dimensional magnetic resonance imaging (4D-MRI) is a potential candidate because of its superior soft tissue contrast and the lack of ionizing radiation compared to 4D-CT, albeit limited efficacy, low efficiency, and inconsistent contrast.[10] These limitations of 4D-MRI can be circumvented by magnetic resonance fingerprinting (MRF)[11], a recent developed

technique for the efficient estimation of MR parameters, such as T1, T2 and proton-density (PD). MRF has the ability to simultaneously acquire quantitative multi-parametric maps in a single scan. These quantitative MR parametric maps have been investigated for diagnosis, tissue characterization, imaging biomarkers, patient follow-up, prognostication, patient management, therapeutic assessment and therapy design.[12-15] Applications of MRF in moving organs have been investigated, including liver, cardiac, and moving brains, which usually involve breath-hold or motion correction strategies. Motion resolved and motion corrected MRF applications in the heart with retrospective binning of the data in different cardiac phases have been investigated.[16,17] However, the application of MRF in abdominal cancer and radiotherapy is limited.

It is therefore highly desired to develop 4D-MRF to improve the efficiency and consistency of radiotherapy motion management. We have recently proposed a continuous MRF acquisition strategy together with retrospective dictionary matching algorithm to track the respiratory motions of the abdomen, dubbed time-resolved MRF (TR-MRF).[18] In this study, we aim to evaluate the effect of different acquisition schemes on the fidelity of TR-MRF using a 4D digital human phantom in a hope to optimize the efficacy of TR-MRF.

2. Materials and method

2.1 Simulation of TR-MRF acquisition

Four-dimensional motions were simulated using the extended 4-dimensional (4D) cardiac-torso (XCAT) phantom.[19-21] The maximum amplitude of diaphragm motion of the 4D XCAT phantom was set to 2.0 cm in the cranial-caudal direction and 1.2 cm in the anterior-

posterior direction. A spherical tumor with diameter of 3.0 cm was added to the liver. Voxel size of XCAT images was set to 1.67 mm isotropic. Irregular breathing of the XCAT phantom in the course of TR-MRF acquisitions was simulated with random amplitude of 0.5 to 2 cm and respiratory period of 3 to 5 s. T1, T2 and PD maps at different respiratory phases were subsequently generated using the values in the literature.[22-24]

TR-MRF acquisition using inversion-recovery unbalanced fast imaging with steady-state free precession sequence[25] and spiral readout was simulated using the extended phase graph algorithm[26] and non-uniform fast Fourier transform.[27] A variable density spiral-in-spiral-out readout trajectory with acquisition window of 8.4 ms and acceleration factor = 58.4 was used. The trajectory was rotated by a golden angle of 222.5^{o} after each dynamic. The pseudorandomized FA varied from 0 to 60^{o} and TR varied from 19 to 21 ms, number of dynamics = 1000, and the number of repetitions range from 1 to 15.

In performing multiple repetition of MRF, three different acquisition strategies could be used were (Figure 1): (1) triggered acquisition with variable delay between MRF repetitions to allow the next acquisition to start at different respiration phase; and continuous acquisition (2) without, and (3) with 5-second delay between MRF repetitions.

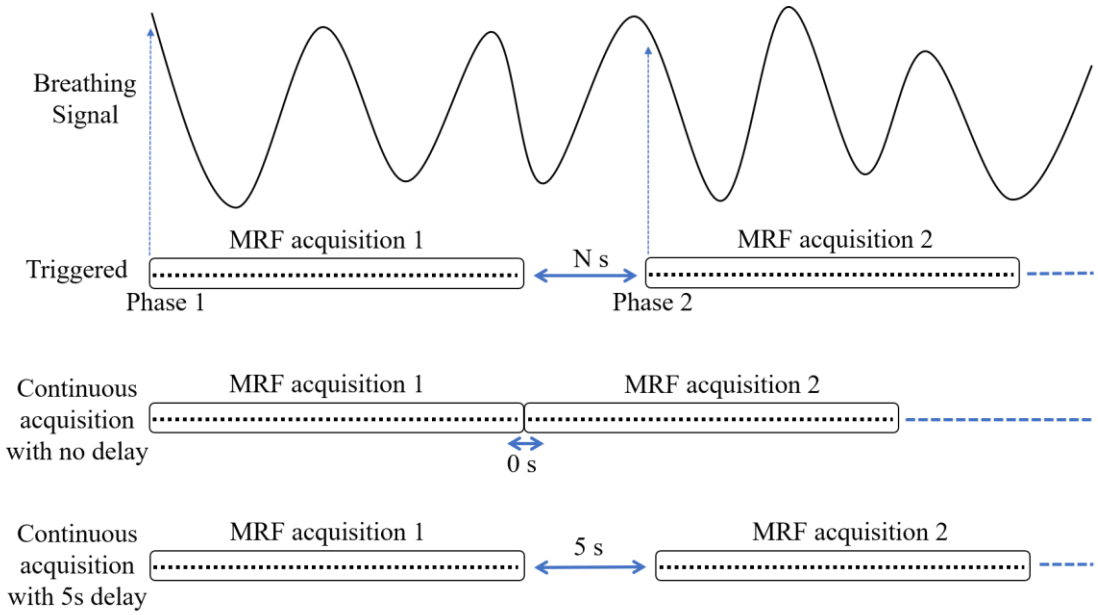

Figure 1: Illustration of different acquisition scheme for TR-MRF. In triggered acquisition, every MRF acquisition starts at different respiratory phases. In continuous acquisition, a 0 or 5 seconds gap between different MRF was simulated. The box represents each MRF acquisition.

2.2 Retrospective reconstruction for motion tracking

The conventional MRF algorithm for the estimation of MR parametric map is known as dictionary matching, whereby the reconstructed dynamic MRF maps are matched to a precalculated dictionary that contains the theoretical signal evolution of all plausible biological tissues [11]. This algorithm only works in the absence of motion. We have therefore proposed TR-MRF to address this issue such that the MR parametric maps at different respiratory phases could be retrospectively obtained[18]. Because the fidelity of TR-MRF reconstruction depends on the number of dynamic MRF maps suitable for dictionary matching of a given respiratory phase[25], we aimed to investigate this relation in the current study.

Phase sorting was used in this study. Specifically, different respiratory phases were identified by evenly partitioning the time between two end of exhalation (EOE) points for each

breathing cycle. Given the respiratory patterns of the XCAT phantom, the respiratory phase to which each dynamic TR-MRF map corresponds can be retrospectively identified. The dynamic TR-MRF maps from different repetitions that fell into the same interval of a given respiratory phase were used in the estimation of MR parametric maps via dictionary matching. In order to study the impact of number of respiratory phases used for reconstruction, a respiratory cycle was first divided into 5~20 phases of the same duration for 10 MRF repetitions. The resulted MRF maps were analyzed.

2.3 Evaluation of the quality of MR parametric maps

MR parametric maps obtained from different acquisition scheme for different respiratory phases were evaluated. Assessment of the T1 and T2, and signal-to-noise-ratio (SNR) of the tumor and liver, tumor-to-liver contrast-to-noise ratio (CNR), absolute difference in motion amplitude, error in the amplitude of diaphragm motion (DME) and tumor volume error (TVE) were performed. The DME is defined as:

$$\mathrm{DME} = \left|\frac{Motion_{TR\ MRF} - Motion_{4D\ XCAT}}{Motion_{4D\ XCAT}}\right| \times 100\%, \quad [1]$$

where $\mathrm{Motion}_{\mathrm{TR\text{-}MRF}}$ and $\mathrm{Motion}_{\mathrm{4D\text{-}XCAT}}$ are the maximum diaphragm motion amplitude between end of inhalation and end of exhalation measured from MR parametric maps and the digital phantom, respectively. The TVE is defined as:

$$\mathrm{TVE} = \left|\frac{Volume_{TR\ MRF} - Volume_{4D\ XCAT}}{Volume_{4D\ XCAT}}\right| \times 100\%, \quad [2]$$

where $\mathrm{Volume}_{\mathrm{TRMRF}}$ and $\mathrm{Volume}_{\mathrm{4DXCAT}}$ are the contoured tumor volume measured from MR parametric maps and the digital phantom, respectively. The tumor volumes were contoured manually from MR parametric maps and digital phantom over 5 respiratory phases between end of exhalation and end of inhalation.

2.4 In-vivo experiment

Three healthy volunteers were recruited to evaluate our newly proposed TR-MRF with both IRB approval and informed consent form obtained. MRI experiments were performed using a 3T human MRI scanner (Achieva TX, Philips Healthcare) with 8-channel torso coil for signal reception. The acquisition matrix = 256 x 256, in-plane resolution = 1.17 x 1.17 mm^2, and slice thickness = 5 mm. The TR-MRF images were acquired in sagittal direction. All sequence and imaging parameters were the same as those described in Section 2.1. A respiratory belt was used to record the breathing signal from volunteers for the retrospective sorting. Triggered acquisition with variable delay between MRF repetitions was performed. It took 13.2 seconds for a single MRF repetition and approximately 3 minutes for a single slice TR-MRF acquisition.

3. Results

3.1 The effect of the number of MRF dynamics on dictionary matching fidelity

MR parametric maps obtained from retrospective dictionary matching using different number of MRF dynamics are shown in Figure 2 and assessments of them in Figure 3. The TVE and DME for T1 and T2 generally increase as the number of MRF dynamics used for retrospective dictionary matching decreases. Notice the TVE and DME of T1 remains respectively below 6% and 2% up to a total of 400 and 600 MRF dynamics. The relation between the number of MRF dynamics available for retrospective dictionary matching and the number of MRF repetitions was also investigated. An apparent logarithm-like relation was

observed. For triggered method with irregular breathing, around 600 unique dynamics on average could be obtained from 10 MRF repetitions as shown in Figure 3E and 3F. For T1 map, the liver SNR, tumor SNR and tumor CNR show a decreasing trend as the number of MRF dynamics used for dictionary matching decreases. For T2 map, the liver SNR decreases then increases, tumor SNR shows an increasing trend and tumor CNR decreases then increases. The mean absolute error of the T1 and T2 of tumor, and the mean absolute error of the T1 of liver show an increasing trend while the mean absolute error of the T2 of liver increases then decreases. All image quality measurements of MRF images simulated with different number of dynamics are shown in Figure 4.

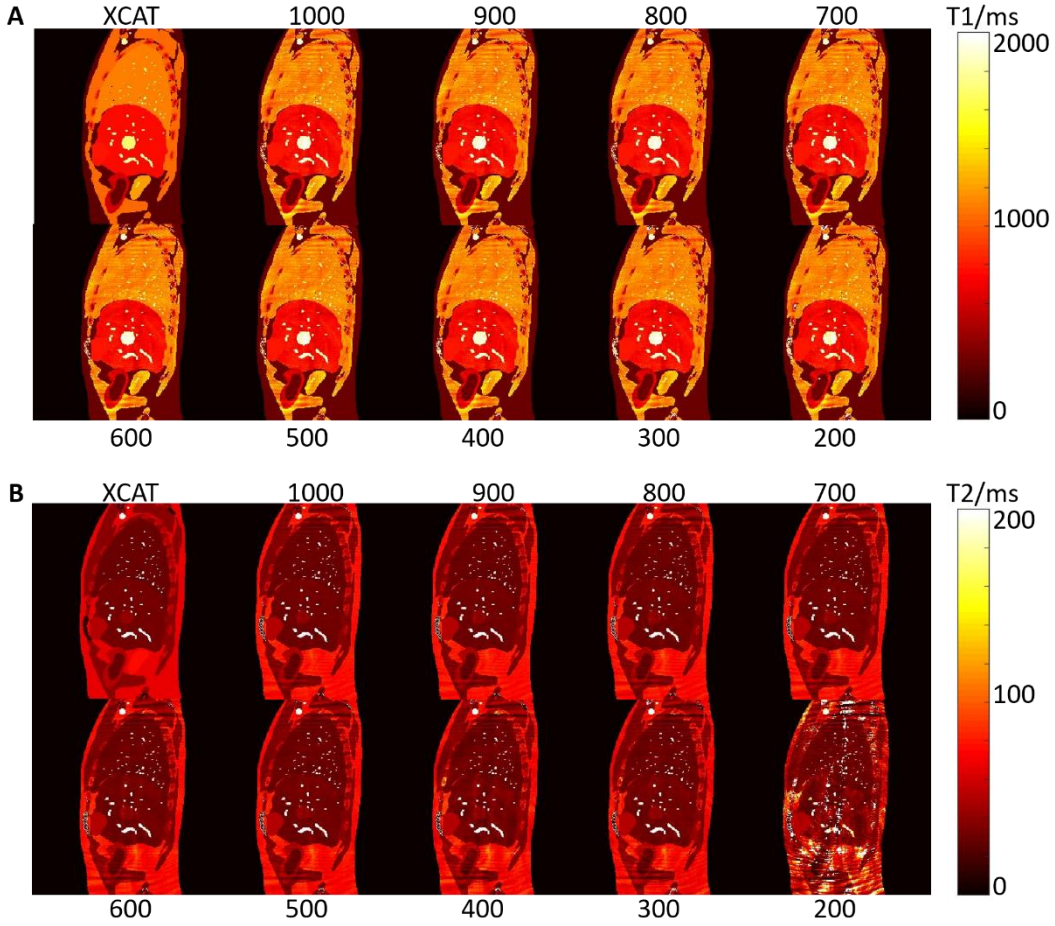

Figure 2: The **(A)** T1 and **(B)** T2 maps obtained from retrospective dictionary matching of different number (1000 to 200) of MRF dynamics. The ground truth from XCAT are also shown.

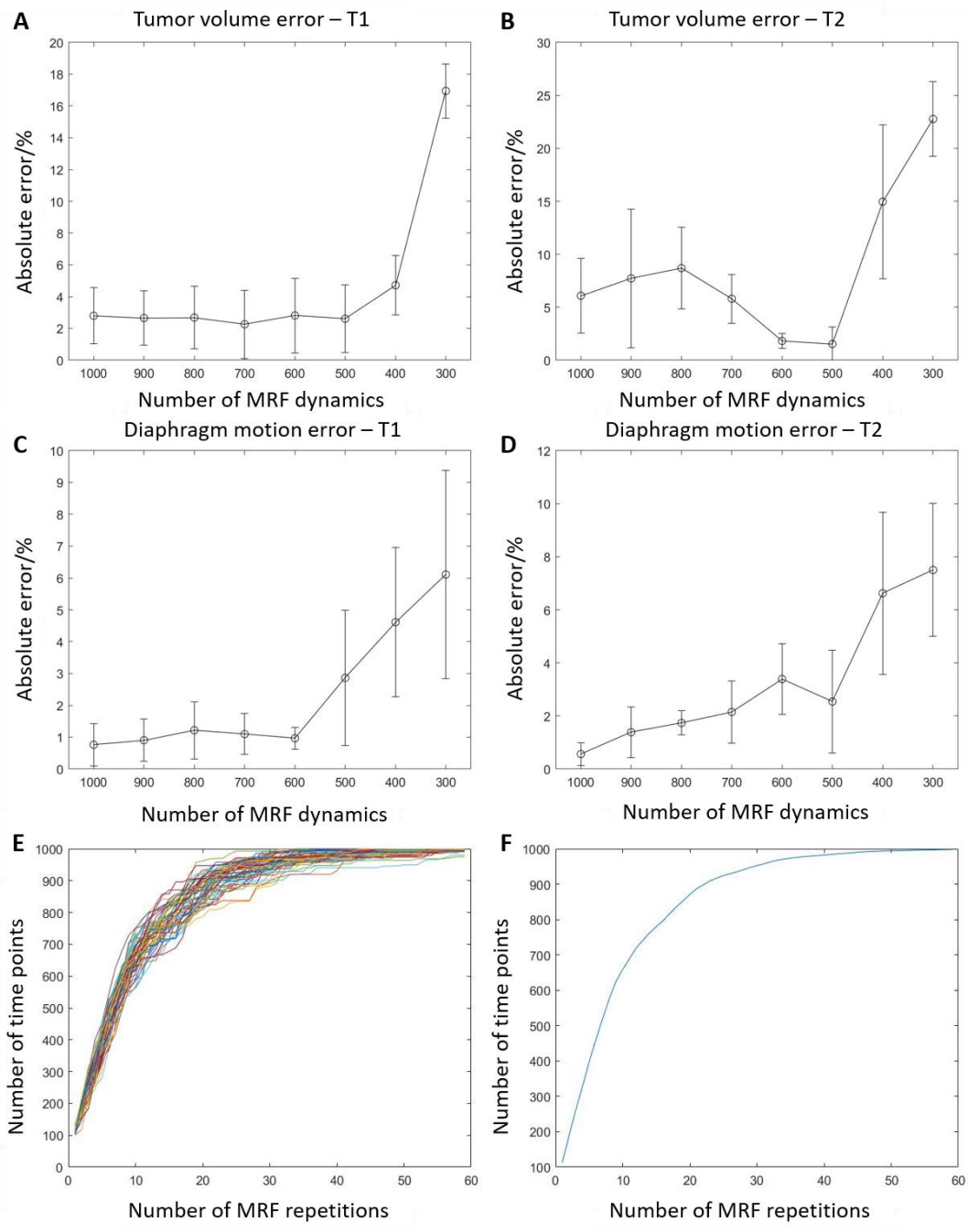

Figure 3: The TVE of **(A)** T1 and **(B)** T2, DME of **(C)** T1 and **(D)** T2 as a function of the number of MRF dynamics available for retrospective dictionary matching. Black circles represent the average of the measurement from all respiratory phases. The error bar is the standard deviation of the measurements. The different simulations showing the relation between the number of unique MRF dynamics **(E)** available for retrospective dictionary matching and the number of MRF repetitions, and **(F)** is the averaged curve from (E).

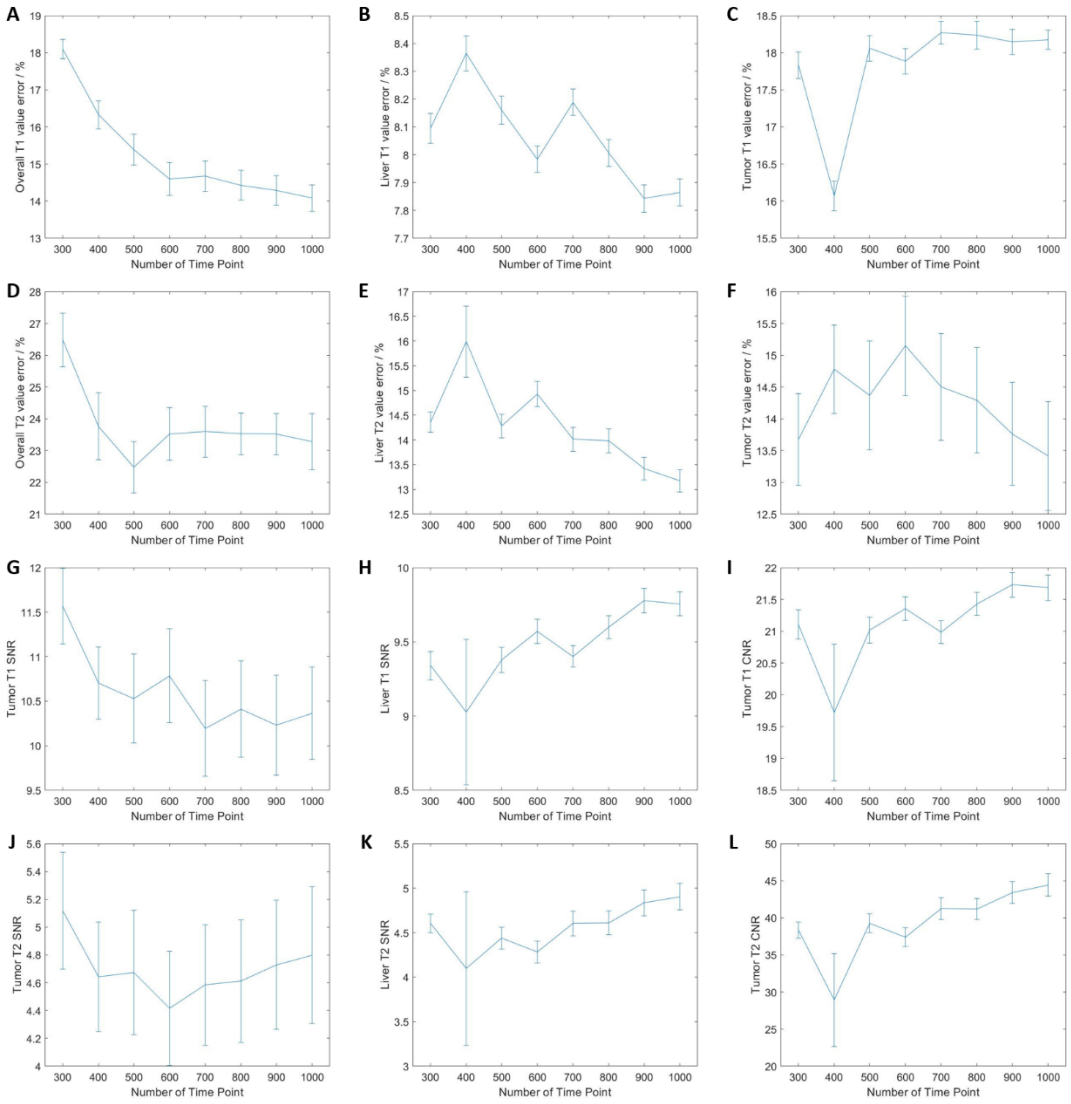

Figure 4: Image quality indexes of the MR parametric maps obtained from TR-MRF for different number of MRF dynamics.

3.2 The effect of TR-MRF acquisition scheme on dictionary matching fidelity

TR-MRF were simulated 100 times for each number of MRF repetitions and TR-MRF acquisition scheme. The error of overall T1 and liver T1, SNR of liver on T1 and T2 maps, and SNR of tumor on T1 map from triggered TR-MRF is significantly better compared to continuous acquisition (p-value < 0.05). The other image quality indexes have no significant difference between the triggered method and the other two continuous acquisition schemes. All image quality indexes exhibit no significant difference (p-value >0.05) between the two

continuous acquisition schemes. The image quality indexes measurement results are shown in Figure 5 and Figure 6.

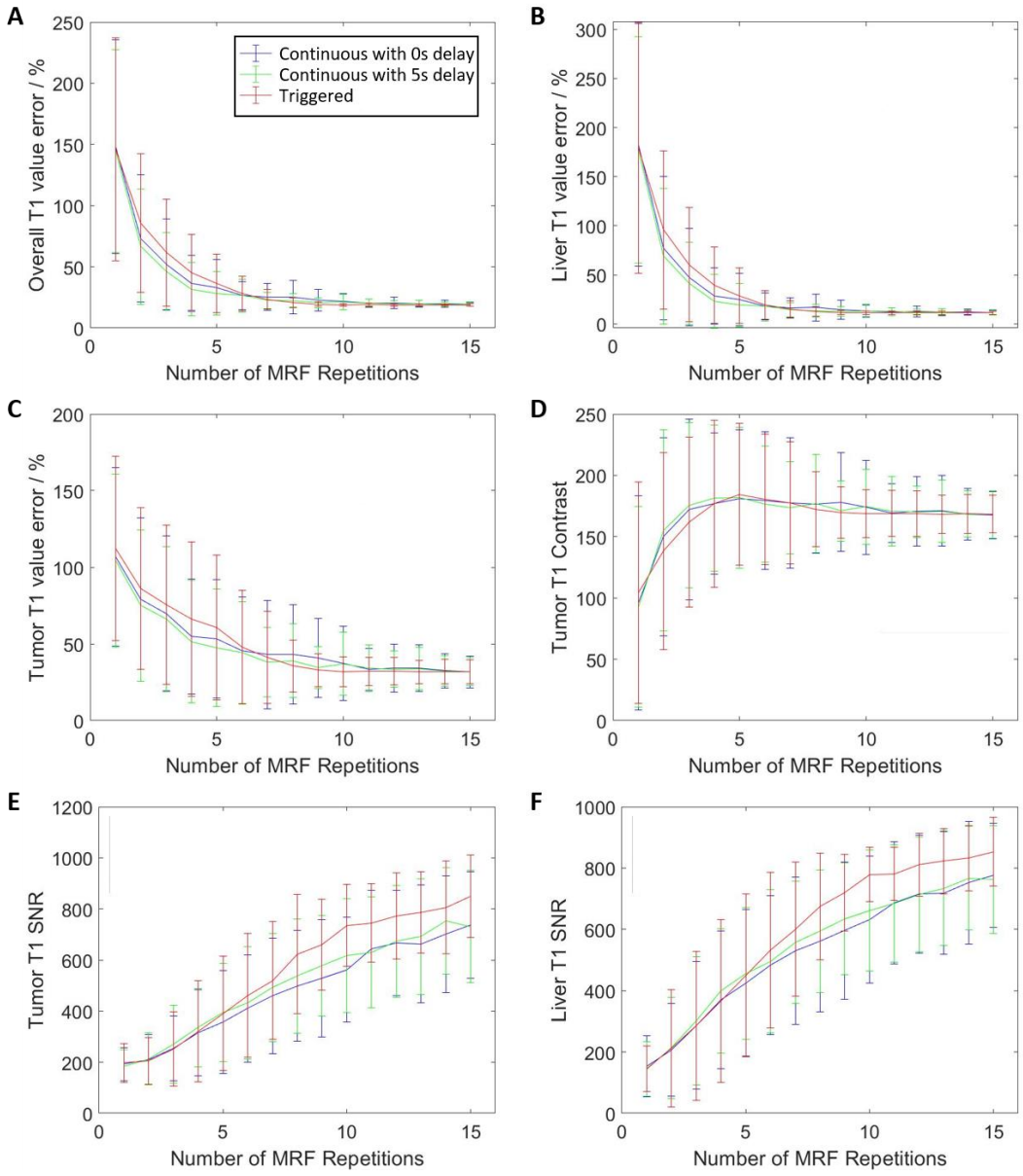

Figure 5: The different image quality indexes of T1 map estimated from different TR-MRF acquisition schemes.

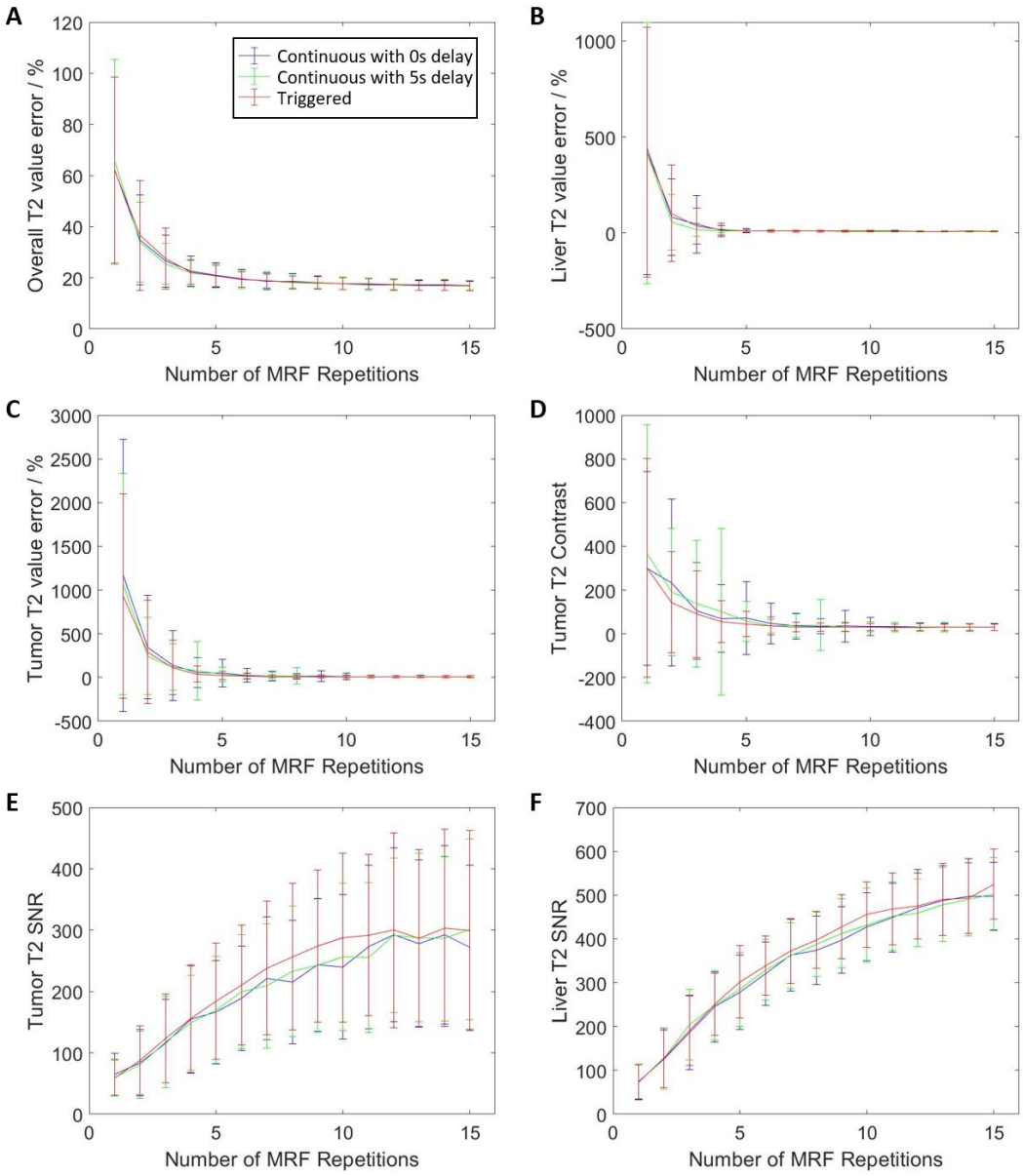

Figure 6: The different image quality indexes of T2 map estimated from different TR-MRF acquisition schemes.

3.3 The influence of number of respiratory phases on image quality

The respiratory cycle was divided equally into 5~20 phases (corresponds to around 80~20 timepoints in each bin) for 10 MRF repetitions of the triggered method with irregular breathing to study the influence of number of phases on the image quality. The reconstructed

images were compared with the XCAT reference images for image quality assessment. The image quality analysis results are shown in Figure 6 and 7. An example of T1 MRF maps reconstructed from different number of phases is show in Figure 8.

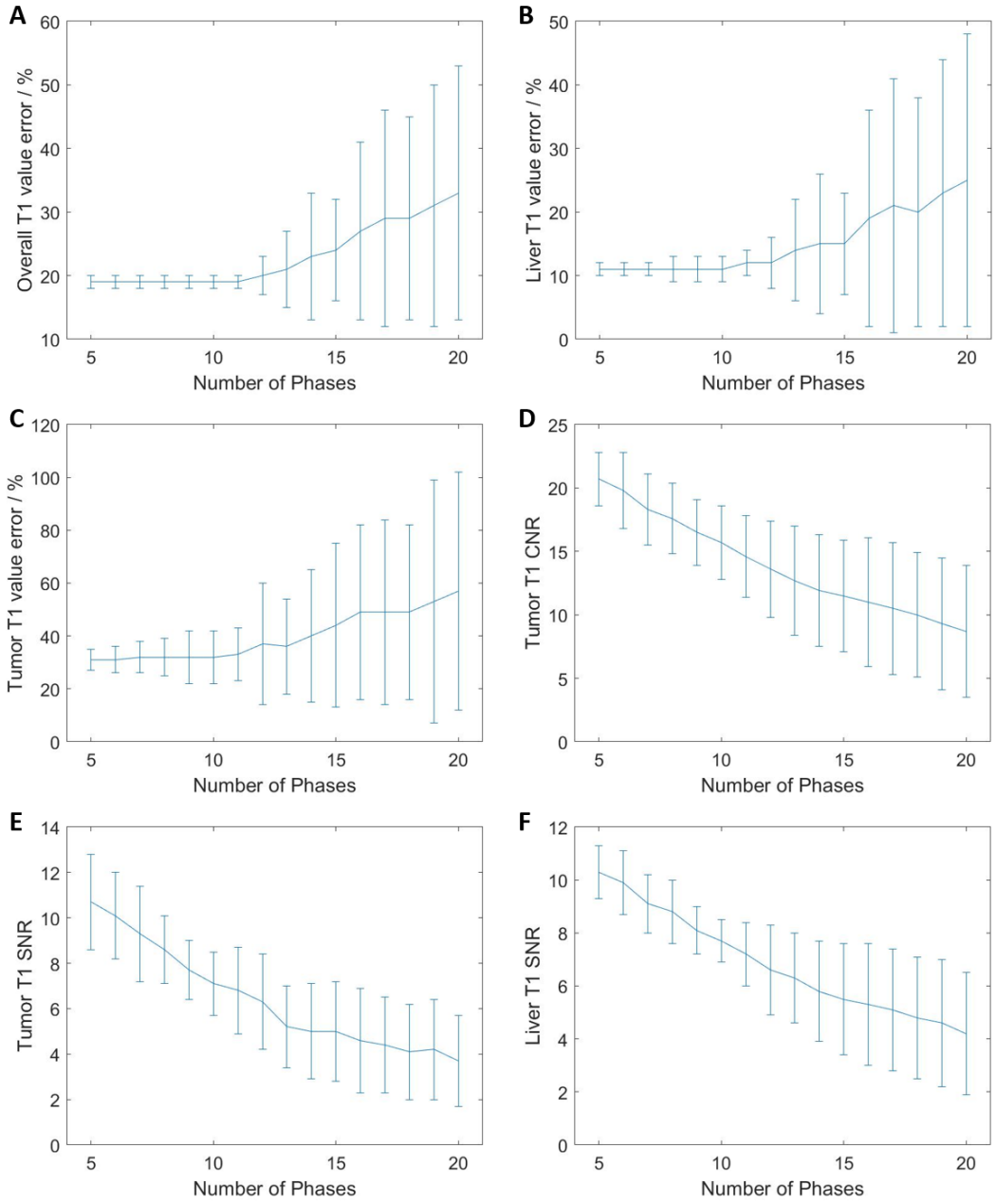

Figure 7: The different image quality indexes of T1 map estimated from different number of TR-MRF respiratory phases.

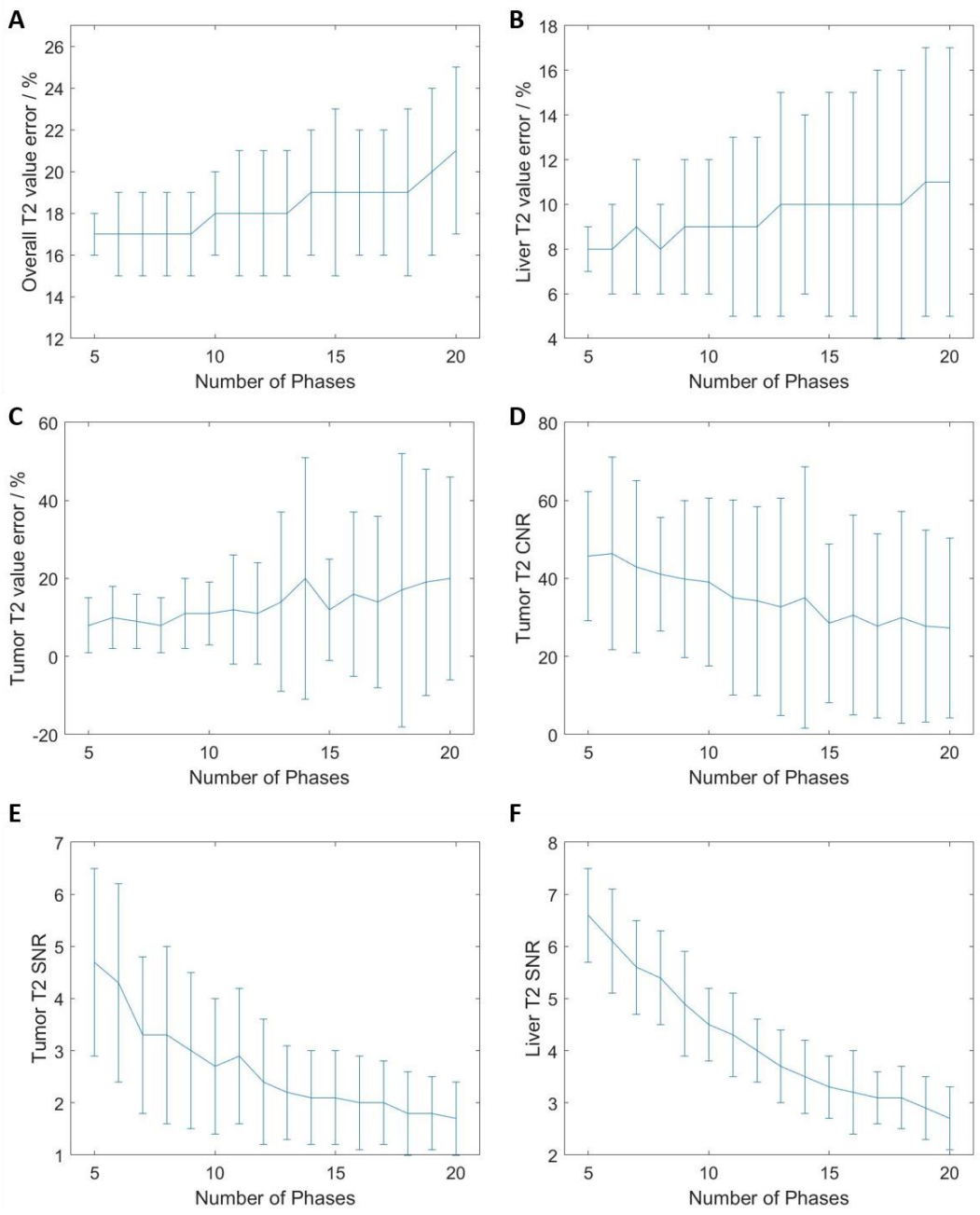

Figure 8: The different image quality indexes of T2 map estimated from different number of TR-MRF respiratory phases.

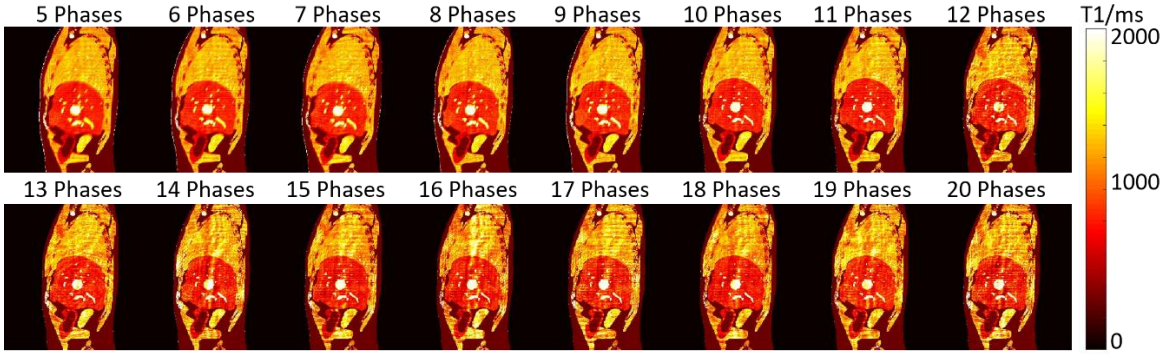

Figure 9: An example of T1 map estimated from different number of TR-MRF respiratory phases with 10 MRF repetitions.

3.4 In-vivo TR-MRF with healthy volunteers

The triggered TR-MRF method was successfully implemented and performed on three healthy volunteers. T1, T2 and PD maps of a representative volunteer are shown in Figure 10. The SNR of liver on T1, T2, and PD maps are 9.0 ± 1.7, 3.0 ± 0.7, 10.7 ± 1.7 respectively.

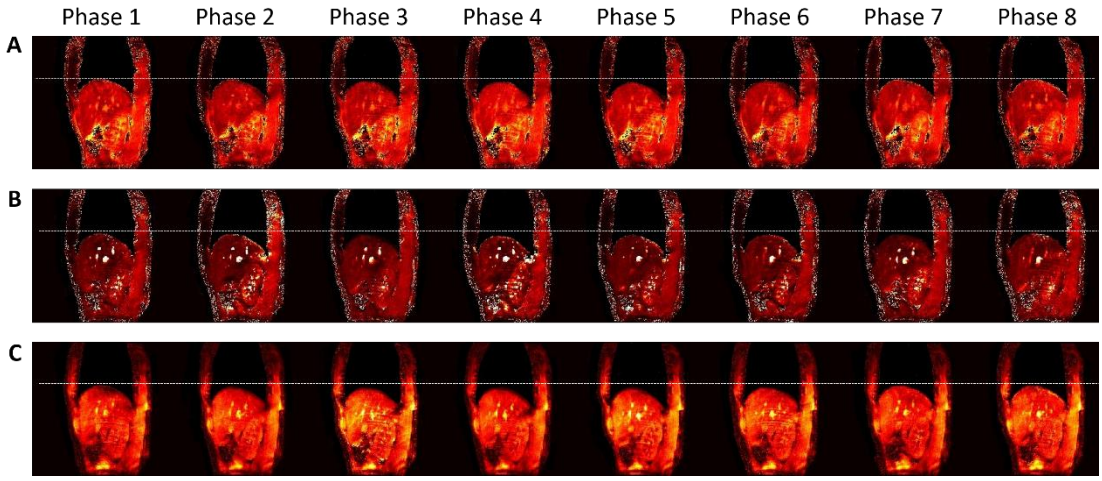

Figure 10: T1 (A), T2 (B), and PD (C) maps of 8 phases of respiration in the sagittal plane of a representative healthy volunteer. Dashed lines are added to facilitate the visualization of the respiratory motion.

4. Discussion

In this study, we investigated different acquisition schemes to generate TR-MRF maps using XCAT phantom and tested an optimal strategy on health volunteers. As far as we know, this is the first study to investigate the acquisition schemes of TR-MRF technique. We also investigated the influence of different number of dynamics and different respiratory phases used for reconstruction on image quality. The key finding of our study is that the quality of T1 and T2 maps generally increase with the number of dynamics.

Considering the most important advantage of TR-MRF technique over the current available 4D-MRI techniques is the quantitative T1 and T2 maps, TR-MRF may potentially be useful for radiotherapy applications where the absolute values of T1 and T2 are important, including tissue classification, longitudinal follow-up, and cross-center comparison. It can be seen in Figure 4 that T1 and T2 errors increase as dynamics decrease. As a result, as many as possible dynamics should be acquired to take full advantages of TR-MRF for these kinds of applications. In terms of motion management application, the motion trajectories measured on MRF maps reconstructed using 600 dynamics show good agreement with motion trajectories measured on standard XCAT images. Both DMAE and TVE stay stable and then shows increasing trend as dynamics decrease in T1 maps as shown in Figure 3. We can conclude that using 600 or more dynamics for reconstruction is acceptable which will yield an average error of less than 5% for these two measurements. It corresponds to around 10 MRF repetitions, which takes around 2 mins scanning time, according to Figure 3F.

Among three different acquisition methods, triggered method showed better performance in terms of certain image quality indexes than the other two methods while the other two

methods showed no significant difference between them. The triggered method could potentially increase the number of unique MRF dynamics in each respiratory phase and improve the image quality by virtue of adjusting the respiratory phase by which each MRF repetition is triggered. The major disadvantage pertains to longer total acquisition time due to varying delay between MRF repetitions. For continuous acquisition with or without delay, the advantage is shorter total acquisition time at the expense of less accurate quantitative maps. We therefore chose the triggered method for volunteer study for its higher fidelity in the estimation of MR parametric maps. The continuous acquisition with 0s gap method can save around 17 mins for a 20 slices TR-MRF acquisition compared to the other two methods and the triggered method requires additional manual efforts. Further in vivo studies are needed to determine the optimal acquisition method for clinical practice. The number of unique dynamics plays an important role in the accuracy of MRF quantitative maps. For the case of triggered MRF acquisition with 10 MRF repetitions during irregular breathing, the total number of unique dynamics for different respiratory phases remains constant at about 650 out of a total of about 1000 dynamics for each respiratory phase. Our results also showed that the error in the estimation of T1 or T2 remain similar when using only unique dynamics versus all acquired dynamics for retrospective dictionary for the case of triggered MRF acquisition.

Regarding the different number of respiratory phases used for reconstruction, it can be seen in Figure 7and Figure 8 that as the number of respiratory phases used increase, the SNR and CNR decrease and the T1 and T2 errors stays stable until 12 phases and then increase. However, using small number of respiratory phases for reconstruction can results in blurred MRF maps as can be seen in Figure 9 for 5~7 respiratory phases. Therefore, the recommended

number of respiratory phases for a 10 MRF repetition acquisition scheme is 8~12 phases.

The dictionary matching method used in this study was template matching using vector-dot product, the same as the first paper introducing MRF.[11] However, this method could be time consuming and computational expensive. Recent study has demonstrated that fewer dynamics could be used for reconstruction using machine-learning based method.[28] This could be useful for TR-MRF application to improve image quality and reduce the number of dynamics required, thus reducing the scanning time. Another method for the acceleration of the TR-MRF technique is using simultaneous multi-slice technique to acquire multiple TR-MRF slices at the same time. This technique has been implemented in static MRF successfully and therefore, hold great promise to accelerate TR-MRF so that it can be practical in real clinic[29]. Future study will compare different matching methods and their influences on the image quality. Pseudo CT generation from MRI is an important aspect in MR-guided radiotherapy. Conventional MRI images have shown promising results in generating pseudo CT. For example, different convolutional neural networks have been proposed to use different conventional MRI images as input to generate pseudo CT images recently. It is possible that MRF maps can replace the conventional MRI images as the input to the network in a more efficient and more accurate manner as the MRF can provide several quantitative maps without the need for registration, and thus potentially improve the quality of synthetic CT. It is therefore worth exploring the pseudo CT generation from TR-MRF technique in the future. Another aspect for future study is use TR-MRF to generate 4D-MRF maps either by using multi-slice or volume imaging technique and to conduct real patient experiment. Although this simulation study has demonstrated the feasibility of TR-MRF using XCAT phantoms, real patient 4D-MRF may

possesses other challenges including dynamics sorting, data insufficiency, and breathing variation etc. Recently, 3D MRF techniques have been investigated by several groups to accelerate MRF acquisition.[30-35] This could be combined with 4D technique to achieve prospective 4D-MRF in the future.

5. Conclusion

The proposed TR-MRF technique was investigated using three different acquisition methods in computer simulation where the triggered method showed better performance than the continuous acquisition. The triggered method was successfully tested in healthy volunteers.

6. Conflict of interest

The authors have no conflict of interest related to this study.

7. Acknowledgement

This research was partly supported by research grants (NIH R01 EB028324, NIH R01 CA226899, GRF 151021/18M, GRF 151022/19M and HMRF 06173276).

References:

1. Bray F, Ferlay J, Soerjomataram I, Siegel RL, Torre LA, Jemal A. Global cancer statistics 2018: GLOBOCAN estimates of incidence and mortality worldwide for 36 cancers in 185 countries. *CA Cancer J Clin.* 2018;68(6):394-424.
2. Clerici E, Comito T, Franzese C, et al. Role of stereotactic body radiation therapy in the treatment of liver metastases: clinical results and prognostic factors. *Strahlenther Onkol.* 2019.
3. Yang JF, Lo CH, Lee MS, et al. Stereotactic ablative radiotherapy versus conventionally fractionated radiotherapy in the treatment of hepatocellular carcinoma with portal vein invasion: a retrospective analysis. *Radiat Oncol.* 2019;14(1):180.
4. Nugent FW, Qamar A, Stuart KE, et al. A randomized phase II study of individualized stereotactic body radiation therapy (SBRT) versus transarterial chemoembolization (TACE) with DEBDOX beads as a bridge to transplant in hepatocellular carcinoma (HCC). *2017 Gastrointestinal Cancer Symposium; San Fransisco, CA.* 2017:19-21.
5. Wahl DR, Stenmark MH, Tao Y, et al. Outcomes after stereotactic body radiotherapy or radiofrequency ablation for hepatocellular carcinoma. *Journal of Clinical Oncology.* 2016;34(5):452-459.
6. Doi H, Beppu N, Kitajima K, Kuribayashi K. Stereotactic Body Radiation Therapy for Liver Tumors: Current Status and Perspectives. *Anticancer Res.* 2018;38(2):591-599.
7. Haddad MM, Merrell KW, Hallemeier CL, et al. Stereotactic body radiation therapy of liver tumors: post-treatment appearances and evaluation of treatment response: a pictorial review. *Abdom Radiol (NY).* 2016;41(10):2061-2077.
8. Price TR, Perkins SM, Sandrasegaran K, et al. Evaluation of response after stereotactic body radiotherapy for hepatocellular carcinoma. *Cancer.* 2012;118(12):3191-3198.
9. Maturen KE, Feng MU, Wasnik AP, et al. Imaging effects of radiation therapy in the abdomen and pelvis: Evaluating 'innocent bystander' tissues. *Radiographics.* 2013;33(2):599-619.
10. Stemkens B, Paulson ES, Tijssen RHN. Nuts and bolts of 4D-MRI for radiotherapy. *Physics in medicine and biology.* 2018;63(21):21tr01.
11. Ma D, Gulani V, Seiberlich N, et al. Magnetic resonance fingerprinting. *Nature.* 2013;495(7440):187-192.
12. O'Connor JP, Aboagye EO, Adams JE, et al. Imaging biomarker roadmap for cancer studies. *Nat Rev Clin Oncol.* 2017;14(3):169-186.
13. Ma D, Pierre EY, Jiang Y, et al. Music-based magnetic resonance fingerprinting to improve patient comfort during MRI examinations. *Magn Reson Med.* 2016;75(6):2303-2314.
14. Wang CY, Liu Y, Huang S, Griswold MA, Seiberlich N, Yu X. (31) P magnetic resonance fingerprinting for rapid quantification of creatine kinase reaction rate in vivo. *NMR Biomed.* 2017;30(12).
15. Gao Y, Chen Y, Ma D, et al. Preclinical MR fingerprinting (MRF) at 7 T: effective quantitative imaging for rodent disease models. *NMR Biomed.* 2015;28(3):384-394.
16. Hamilton JI, Jiang Y, Eck B, Griswold M, Seiberlich N. Cardiac cine magnetic resonance fingerprinting for combined ejection fraction, T(1) and T(2) quantification. *NMR Biomed.*

2020;33(8):e4323.
17. Jaubert O, Cruz G, Bustin A, et al. Free-running cardiac magnetic resonance fingerprinting: Joint T1/T2 map and Cine imaging. *Magnetic Resonance Imaging.* 2020;68:173-182.
18. Li T, Cui D, Hui ES, Cai J. Time-Resolved Magnetic Resonance Fingerprinting for Radiotherapy Motion Management. *Med Phys.* 2020.
19. Segars WP, Sturgeon G, Mendonca S, Grimes J, Tsui BMW. 4D XCAT phantom for multimodality imaging research. *Medical Physics.* 2010;37(9):4902-4915.
20. Cai J, Chang Z, Wang Z, Paul Segars W, Yin FF. Four-dimensional magnetic resonance imaging (4D-MRI) using image-based respiratory surrogate: a feasibility study. *Med Phys.* 2011;38(12):6384-6394.
21. Liu Y, Yin FF, Chen NK, Chu ML, Cai J. Four dimensional magnetic resonance imaging with retrospective k-space reordering: a feasibility study. *Med Phys.* 2015;42(2):534-541.
22. Chen Y, Jiang Y, Pahwa S, et al. MR Fingerprinting for Rapid Quantitative Abdominal Imaging. *Radiology.* 2016;279:9.
23. Chow AM, Gao DS, Fan SJ, et al. Measurement of liver T(1) and T(2) relaxation times in an experimental mouse model of liver fibrosis. *J Magn Reson Imaging.* 2012;36(1):152-158.
24. Heye T, Yang SR, Bock M, et al. MR relaxometry of the liver: significant elevation of T1 relaxation time in patients with liver cirrhosis. *Eur Radiol.* 2012;22(6):1224-1232.
25. Jiang Y, Ma D, Seiberlich N, Gulani V, Griswold MA. MR fingerprinting using fast imaging with steady state precession (FISP) with spiral readout. *Magn Reson Med.* 2015;74(6):1621-1631.
26. Weigel M. Extended phase graphs: dephasing, RF pulses, and echoes - pure and simple. *J Magn Reson Imaging.* 2015;41(2):266-295.
27. Fessler JA, Sutton BP. Nonuniform fast Fourier transforms using min-max interpolation. *IEEE Transactions on Signal Processing.* 2003;51(2):560-574.
28. Fang Z, Chen Y, Liu M, et al. Deep Learning for Fast and Spatially-Constrained Tissue Quantification from Highly-Accelerated Data in Magnetic Resonance Fingerprinting. *IEEE Trans Med Imaging.* 2019.
29. Ye H, Cauley SF, Gagoski B, et al. Simultaneous multislice magnetic resonance fingerprinting (SMS-MRF) with direct-spiral slice-GRAPPA (ds-SG) reconstruction. *Magn Reson Med.* 2017;77(5):1966-1974.
30. Ma D, Jiang Y, Chen Y, et al. Fast 3D magnetic resonance fingerprinting for a whole-brain coverage. *Magn Reson Med.* 2018;79(4):2190-2197.
31. Amthor T, Doneva M, Koken P, Sommer K, Meineke J, Bornert P. Magnetic Resonance Fingerprinting with short relaxation intervals. *Magn Reson Imaging.* 2017;41:22-28.
32. Liao C, Bilgic B, Manhard MK, et al. 3D MR fingerprinting with accelerated stack-of-spirals and hybrid sliding-window and GRAPPA reconstruction. *Neuroimage.* 2017;162:13-22.
33. Bo Z, Bilgic B, Adalsteinsson E, Griswold MA, Wald LL, Setsompop K. Simultaneous multislice magnetic resonance fingerprinting with low-rank and subspace modeling. *Conf Proc IEEE Eng Med Biol Soc.* 2017;2017:3264-3268.
34. Ma D, Jones SE, Deshmane A, et al. Development of high-resolution 3D MR

fingerprinting for detection and characterization of epileptic lesions. *J Magn Reson Imaging*. 2019;49(5):1333-1346.

35. Cao X, Ye H, Liao C, Li Q, He H, Zhong J. Fast 3D brain MR fingerprinting based on multi-axis spiral projection trajectory. *Magn Reson Med*. 2019;82(1):289-301.